Biomolecular solid state NMR with magic-angle spinning at 25 K

Kent R. Thurber, Robert Tycko *

Laboratory of Chemical Physics, National Institute of Diabetes and Digestive and Kidney Diseases, National Institutes of Health, Building 5, Room 112, Bethesda, MD 20892-0520, USA

ABSTRACT

A magic-angle spinning (MAS) probe has been constructed which allows the sample to be cooled with helium, while the MAS bearing and drive gases are nitrogen. The sample can be cooled to 25 K using roughly 3 L/h of liquid helium, while the 4-mm diameter rotor spins at 6.7 kHz with good stability (±5 Hz) for many hours. Proton decoupling fields up to at least 130 kHz can be applied. This helium-cooled MAS probe enables a variety of one-dimensional and two-dimensional NMR experiments on biomolecular solids and other materials at low temperatures, with signal-to-noise proportional to $1/T$. We show examples of low-temperature ^{13}C NMR data for two biomolecular samples, namely the peptide $A\beta_{14-23}$ in the form of amyloid fibrils and the protein HP35 in frozen glycerol/water solution. Issues related to temperature calibration, spin–lattice relaxation at low temperatures, paramagnetic doping of frozen solutions, and ^{13}C MAS NMR linewidths are discussed.

Published by Elsevier Inc.

1. Introduction

Nuclear magnetic resonance (NMR) experiments are often limited by sensitivity. One very general method to increase the signal for solid state NMR is to cool the sample [1,2]. At temperatures above 1 K and in standard NMR magnets, the nuclear spin polarization at thermal equilibrium is proportional to $1/T$, where T is the temperature. Thus, if we cool the sample to 25 K from room temperature (∼295 K), NMR signals can be increased by a factor greater than 10. Additional improvement in signal-to-noise can be gained by cooling the detection circuit along with the sample [3,4]. Even this smaller enhancement from cooling the detection circuit, but not the sample, was a leap forward in solution NMR technology [4]. In our solid state NMR probe, we use the signal enhancement from cooling the sample, with the future possibility of additional signal-to-noise benefit by cooling the detection circuit.

Cooling a static sample with liquid helium is relatively straightforward [5–11], but cooling with helium while using magic-angle spinning (MAS) has proven more difficult. Several groups have developed MAS probes that use helium gas for both cooling and spinning [12–16]. These designs have had various limitations, including low spinning speed [12,16], low spinning stability [13–15], and high helium consumption. For our application of solid state NMR to study biomolecular systems, we want a large sample volume, and to use two-dimensional (2D) NMR and multiple pulse recoupling techniques that have not yet been demonstrated with these all-helium MAS probes. In particular, to be useful in our studies of biomolecular structure, a low-temperature MAS probe

should have high spinning stability (i.e., MAS frequency fluctuations much less than 1%), must be able to achieve high radio-frequency (rf) field strengths on two or more rf channels for periods greater than 10 ms (e.g., 50 kHz ^{13}C rf fields and 100 kHz ^1H fields), and must have sufficiently low helium consumption that experiments can be run for many consecutive hours at low temperatures.

In this paper, we describe a MAS probe that can cool the sample to 25 K with liquid helium. This probe is designed for experiments at moderate MAS frequencies with relatively large sample volumes. The probe uses room temperature nitrogen as the bearing and drive gas. This enables stable spinning at moderately high MAS frequencies, so that standard multiple pulse and 2D NMR experiments can be performed. Liquid helium consumption at 25 K is approximately 3 L/h, with the 4-mm diameter rotor spinning at 6.7 kHz with good stability (±5 Hz) for more than 12 consecutive hours. We have successfully applied proton decoupling fields up to 130 kHz for 5 ms during dipolar recoupling periods, and 75 kHz for 20 ms during evolution and detection periods of 2D measurements. To demonstrate the capabilities of the probe, we show examples of ^{13}C MAS NMR measurements on two samples, namely amyloid fibrils formed by residues 14–23 of the β-amyloid peptide associated with Alzheimer's disease ($A\beta_{14-23}$) [17] and the protein HP35 in frozen solution [18].

2. Materials and methods

2.1. Probe design

Fig. 1a shows a sketch of the MAS unit. The design is based on a 4 mm outer diameter rotor that is 4.57 cm long. Compared with standard MAS rotor lengths of 3.1 cm or less, the greater rotor
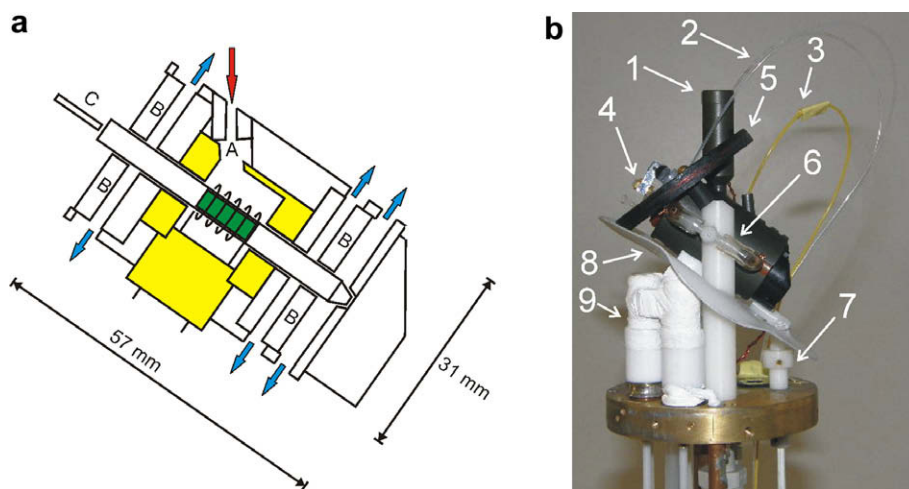
Fig. 1. (a) Cross-section of MAS unit of helium-cooled low temperature solid state NMR probe. Cold helium (red arrow) enters the MAS unit through the tube labeled A. The sample (green) sits in the sample space region defined by two Teflon pieces (yellow), which fit together to hold the NMR coil and separate the helium-cooled sample space from the nitrogen gas. Helium gas exits the sample space in the small gap around the circumference of the rotor. Both the nitrogen gas, used for the air bearings (B) and for spinning, and the helium gas can vent from the MAS unit on either side of each of the bearings (blue arrows). For stable spinning, the rotor requires a "pointer" (C) which acts to dampen vibration of the rotor. (b) Photograph of the probe head, with outer aluminum can removed. Arrows indicate the helium entry tube (1), optical fibers for MAS tachometer (2), fiber optic temperature sensor (3), hinged pointer for stabilizing spinning (4), shim coil (5), bearing gas supply tubes (6), MAS angle adjust rod (7), Teflon baffle (8), tuning and matching capacitors for ^{13}C channel (9). (For interpretation of color mentioned in this figure the reader is referred to the web version of the article.)

length provides increased separation between the helium-cooled sample region and the warmer nitrogen bearing and spinning gas. The rotor drive tip, brass stator, and ceramic bearings are from a Varian 4 mm MAS unit. Liquid helium is fed from a pressurized helium dewar (7–8 psi for low temperatures) through a vacuum-insulated metal transfer line with a needle valve to control helium flow (Janis Research). The transfer tube feeds into a short (5 cm long) segment of Torlon at the top of the sample region. This short section of plastic helps to eliminate excess noise pickup from the helium transfer line, in combination with grounding of the bottom end of the transfer line to the probe body. Cold helium then enters the MAS unit through the hole labeled A in Fig. 1a.

To avoid electrical discharge arcing in the helium gas atmosphere [11], the coil is made with Teflon-coated wire (Alpha Wire Co., 18 gauge wire with 0.25 mm of Teflon insulation, 5 turns, inner diameter 4.7 mm), and the sample space is surrounded by a Teflon insert (shown in yellow in Fig. 1a). This Teflon insert also defines the sample space cooled by the helium. The helium-cooled sample space is mostly closed, but the helium gas can vent around the outer surface of the rotor into the two bearing areas. Then, both the helium gas and the nitrogen gas vent out of the MAS unit on both sides of each bearing (indicated by blue arrows on Fig. 1a). It is important to have a vent for the nitrogen bearing gas on the sample side of the bearings, to avoid warming the sample space with the nitrogen gas. Currently, we are using room temperature nitrogen gas for both the bearing and drive gases. In a future design, cooling of the bearing and drive gas may enable lower sample temperatures or lower helium consumption. At room temperature, this MAS unit achieves MAS frequencies up to $\nu_{MAS} = 10$ kHz. At low temperatures, we have performed most experiments at $\nu_{MAS} = 6.7$ kHz. At 9.4 T, this MAS frequency is high enough for a wide variety of solid state NMR techniques, and is high enough to prevent overlap of MAS sideband signals from natural-abundance ^{13}C of glycerol with other ^{13}C signals (see below). Because room temperature nitrogen gas is used for the bearings and spinning, there is a tradeoff between increasing spinning speed and achieving low temperatures.

Fig. 1b shows a photograph of the probe head. Commercial variable capacitors (Polyflon) are used for tuning and matching of the ^{13}C channel and for matching of the ^{1}H channel, and a home-built cylindrical coaxial capacitor that can be adjusted by moving a Tef-

lon dielectric is used for ^{1}H tuning. Although the current probe design also includes a pair of capacitors for a ^{15}N channel, this third channel was not connected in experiments described below. During experiments, nitrogen purge gas flows continuously into the area of the capacitors, and also into the lower probe body. The outer diameter of the probe body is 88 mm, necessitating removal of the room temperature shims from our 89-mm bore superconducting magnet before the probe can be raised into the magnet. A single internal shim coil was therefore included in the probe to enable shimming. The shim coil consists of 15 turns of 22 gauge wire on a 6 cm diameter form, mounted roughly 2 cm above the center of the rotor, and tilted at a 35° angle to avoid other probe parts. A shim current of roughly 0.65 A was used in the experiments described below, provided by a DC power supply (HP 6236B or GW PPT-3615). RF noise from the shim coil was avoided by using a coaxial lead with the outer conductor grounded to the probe body, and capacitors and RF chokes for filtering. At low temperatures, the shim current was adjusted to minimize the ^{79}Br NMR linewidth for KBr powder (140 Hz) under MAS. The sample volume available (green area in Fig. 1a) is 48 or 82 μl depending on the wall thickness of the rotor. All experiments reported below used a thick-wall (48 μl) rotor except for the data of Fig. 9, which were taken in a thin-wall (82 μl) rotor.

MAS frequencies were monitored with a fiber optic tachometer. A fiber optic temperature sensor (Neoptix model $T1$) in contact with the MAS unit was used to monitor liquid helium flow and as a rough indicator of sample temperature. Sample temperatures were determined more precisely as described below.

2.2. Sample preparation

An Aβ$_{14–23}$ peptide sample (amino acid sequence HQKLVFFAED) with uniform ^{15}N and ^{13}C labeling of V18 and A21 was synthesized and fibrillized as previously described [17]. For measurements described below, 2.7 mg of fibrils were mixed into 25 μl of glycerol/water (3:2 ratio by volume) in the MAS rotor, with 160 μM DyED-TA. A similar sample was also prepared without DyEDTA. Previous solid state NMR measurements have shown that Aβ$_{14–23}$ fibrils have a highly ordered antiparallel β-sheet structure, with intermolecular hydrogen bonding of V18 and A21 within the β-sheets [17].

An HP35 protein sample (amino acid sequence LSDEDFKAVFGMTRSAFA NLPLWKQQNLKKEKGLF, representing residues 42–76 of the 76 residue chicken villin headpiece [19]) with uniform ^{15}N and ^{13}C labeling of V50, A57, and L69 was synthesized as previously described [18]. Several samples were prepared by dissolving 0.55–0.79 mg of HP35 in 48 μl of glycerol/water (1:1 or 3:2 ratio by volume) with various DyEDTA concentrations (for Fig. 5), or 1.3 mg of HP35 in 80 μl of glycerol/water (1:1 by volume) (for Fig. 9). HP35 has a three-helix-bundle structure, with residues 44–50, 55–58, and 63–72 forming the α-helices [19,20]. Previous solid state NMR measurements have shown that this structure is retained in frozen glycerol/water in the absence of chemical denaturants [18].

An additional test sample was prepared by dissolving 2.2 mg of ^{13}CH$_3$-labeled sodium acetate in 47 μl of glycerol/water (4:3 ratio by volume) with 200 μM DyEDTA.

Samples were frozen before loading into the MAS probe by immersion of the rotor in liquid nitrogen. To ensure that the samples stayed frozen, the probe was precooled under MAS conditions with a KBr powder sample, before the rotors were exchanged. Glycerol/water solutions were used to avoid water crystallization. These solutions have glass transition temperatures of approximately 190 K. DyEDTA was added to the samples to accelerate ^{1}H spin–lattice relaxation, as discussed below.

3. Results

3.1. Signal enhancement at low temperatures

Fig. 2a shows one-dimensional (1D) ^{13}C NMR spectra of sodium 2-^{13}C-acetate in frozen glycerol/water solution with 200 μM DyEDTA at a series of temperatures. These spectra were obtained at v_{MAS} = 7.00 kHz, using 1.5 ms ^{1}H–^{13}C cross-polarization periods with 48 and 62 kHz ^{13}C and ^{1}H rf fields, respectively, and using proton decoupling with a 105 kHz field. Chemical shift referencing in Fig. 2a and all subsequent figures is based on the natural-abundance glycerol ^{13}C lines at 62.9 and 72.7 ppm, after calibration of the glycerol peaks with a sample containing both frozen glycerol/water and 1-^{13}C-alanine solid powder used for reference at 177.96 ppm. The ^{13}C NMR signals in Fig. 2a increase strongly as the temperature is lowered. As shown in Fig. 2b, the integrals of the ^{13}C peaks follow a $1/T$ dependence between sample temperatures of 25 and 79 K. This temperature dependence is consistent with signal enhancement primarily from increased spin polarization at low temperatures, with negligible contribution from in-
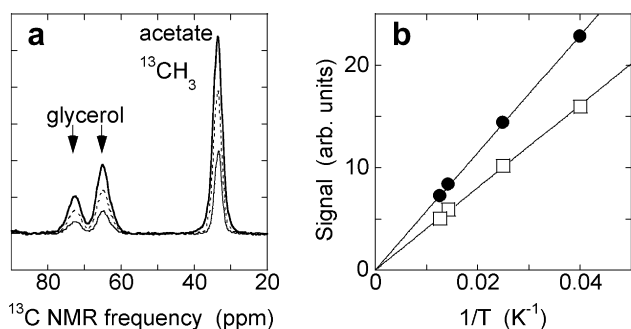
creased quality factor (Q) of the rf circuit, or change in cross-polarization efficiency. In agreement with this, we observed that the Q for the ^{13}C RF channel of the probe increases by only roughly 10% on cooling the sample from room temperature to 25 K. Direct temperature measurement shows that the tuning capacitor of the probe is at 267 K during low temperature operation. For our current ^{13}C receiver with room temperature pre-amplifier, the ^{13}C noise figure is 1.9 db, corresponding to a 160 K noise temperature. Additional sensitivity enhancement would be expected if the entire RF circuit and pre-amplifier were cooled further.

3.2. 2D ^{13}C–^{13}C NMR spectroscopy at 25 K

Fig. 3a shows a 2D ^{13}C–^{13}C spectrum of the Aβ$_{14–23}$ fibril sample, obtained at v_{MAS} = 6.70 kHz with radio-frequency-driven recoupling (RFDR) [21] and 100 kHz CW proton decoupling during the 1.2 ms mixing period, and with 75 kHz two-pulse phase modulated (TPPM) proton decoupling [22] during the evolution and detection periods. This spectrum shows intra-residue crosspeaks for the isotopically labeled V18 and A21 residues with good signal-to-noise after only 2048 total scans (3.5 h total experiment time with a 6 s recycle delay). Fig. 3b shows a 2D ^{13}C–^{13}C spectrum of the same sample, obtained with a 500 ms spin diffusion period as the mixing period and also acquired with a total of 2048 scans. This spectrum shows inter-residue crosspeaks between V18 and A21, which arise from the intermolecular proximity of these residues in an antiparallel β-sheet [17], in addition to the intra-residue crosspeaks. Together, Fig. 3a and b demonstrate that double-resonance techniques that are commonly applied in biomolecular solid state NMR can be carried out successfully and yield high-quality data at low temperatures with this MAS probe, under the same pulse sequence conditions as might be employed in room temperature experiments.

^{13}C NMR linewidths in Fig. 3 are 3–6 ppm. At room temperature, hydrated Aβ$_{14–23}$ fibrils exhibit 1.0 ppm ^{13}C NMR linewidths [17]. We attribute this difference primarily to motional narrowing at room temperature, due to a combination of molecular motions of peptide molecules in the fibrils and motions of solvent molecules. At low temperatures, these motions are completely quenched, producing static disorder that results in distributions of ^{13}C chemical shifts for each labeled site. Related increases in linewidths in frozen samples have been reported by other groups [23,24]. Linewidths in Fig. 3 are not affected by the DyEDTA dopant, as verified by additional measurements on undoped Aβ$_{14–23}$ fibrils at low temperatures.

3.3. Homonuclear dipolar recoupling at 25 K

Fig. 4 shows a measurement of intra-residue ^{13}CO–^{13}C$_\alpha$ magnetic dipole–dipole couplings for A21 in the Aβ$_{14–23}$ fibril sample using the SEASHORE frequency-selective dipolar recoupling technique [25]. These data were taken using only 32 scans per point, with v_{MAS} = 6.560 kHz and a 152.4 μs chemical shift evolution period (i.e., one rotor period) between double-quantum recoupling blocks for frequency selectivity. The POST-C7 sequence was used for recoupling [26]. A 130 kHz proton decoupling field was applied during POST-C7 blocks. Clear oscillations are seen in the data, which by comparison to simulations provide a single bond distance of 1.51 ± 0.05 Å. This is in good agreement with the value of 1.53 Å for crystalline L-alanine [27]. The data are plotted as $(A_O + A_\alpha)/(A_O − A_\alpha)$, where A_O and A_α are the integrals of the carbonyl peak (overlapping V18 and A21) and the A21 C$_\alpha$ peak, with selective excitation of carbonyl spin polarization before SEASHORE recoupling as previously described [25]. Simulations in Fig. 4 are offset by ~0.5 from the experimental data because of the contribution of the V18 carbonyl (which is not recoupled in these experiments)
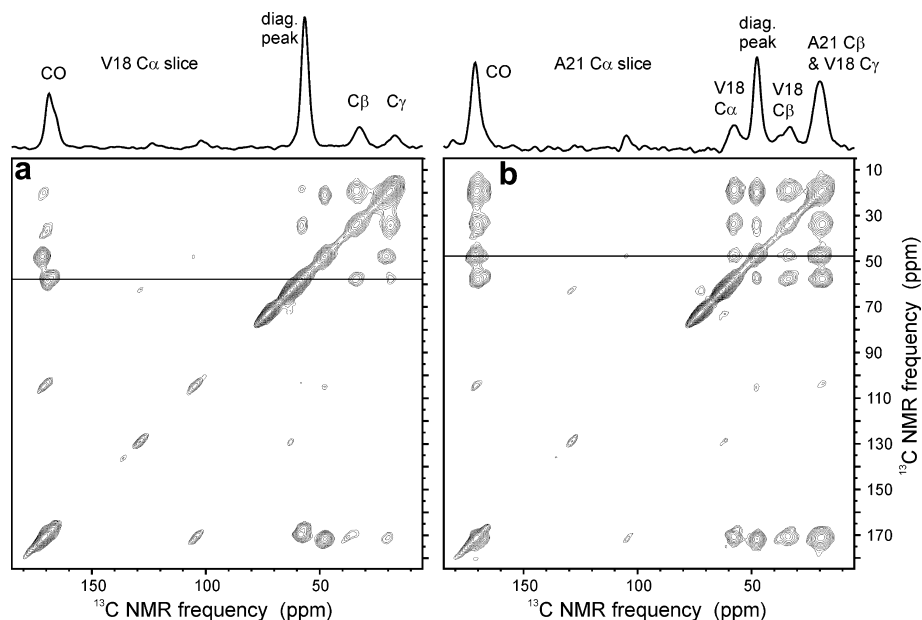

Fig. 2. (a) ^{13}C MAS NMR spectra of ^{13}CH$_3$-labeled sodium acetate dissolved in frozen glycerol/water with 200 μM DyEDTA, recorded at 25 K (heavy solid line), 40 K (dashed line), and 79 K (thin line). Spectra are on the same vertical scale. Each spectrum is the result of four scans, recorded with 7.00 kHz MAS, ^{1}H–^{13}C cross-polarization (1.5 ms), and 105 kHz ^{1}H decoupling. Recycle delays were 33–56 s, sufficient for complete spin–lattice relaxation between scans. (b) Peak integrals as a function of inverse temperature (● acetate CH$_3$, □ glycerol). Lines show linear fits, indicating a linear dependence of the cross-polarized ^{13}C NMR signal on $1/T$.

Fig. 3. (a) 2D ^{13}C–^{13}C NMR spectrum of Aβ_{14-23} fibrils with uniform ^{15}N and ^{13}C labeling of V18 and A21, acquired at 25 K with RFDR recoupling in the 1.2 ms mixing period. A 1D slice is shown at the V18 $^{13}C_\alpha$ chemical shift, with intra-residue crosspeaks labeled. (b) 2D ^{13}C–^{13}C NMR spectrum with spin diffusion in the 500 ms mixing period. A 1D slice is shown at the A21 $^{13}C_\alpha$ chemical shift, with inter-residue and intra-residue crosspeaks labeled. Each spectrum was acquired in 3.5 h (2048 total scans, recycle delay 6 s, 6.7 kHz MAS).
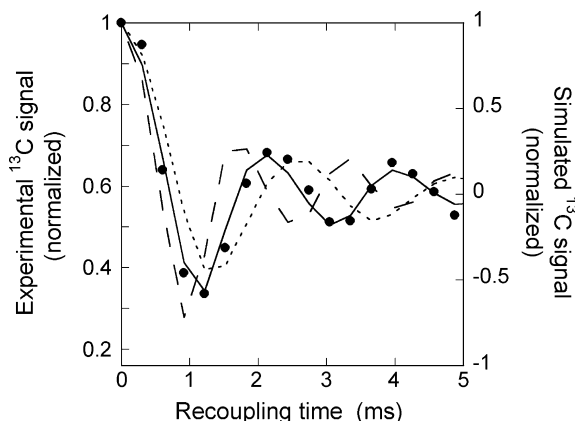

Fig. 4. Frequency-selective dipolar recoupling of A21 ^{13}CO and $^{13}C_\alpha$ spins in Aβ_{14-23} fibrils at 25 K, using the SEASHORE technique with POST-C7 double-quantum recoupling. Dashed, solid, and dotted lines are simulations for two-spin systems with 1.40, 1.50, and 1.60 Å internuclear distances, including anisotropic chemical shifts. A 5 ms exponential decay was applied to the simulated curves to match the damping of the experimental oscillations.

to the experimental A_O values. These results demonstrate that high-power proton decoupling is feasible under MAS at 25 K, allowing observation of sizeable signal oscillations under double-quantum recoupling.

3.4. 2D ^{13}C–^{13}C NMR of a protein solution at 25 K

Fig. 5a shows a 2D ^{13}C–^{13}C spectrum of HP35 in frozen glycerol/water with 400 μM DyEDTA, at a protein concentration of 4 mM (0.19 μmol of HP35), recorded at 25 K with v_{MAS} = 6.70 kHz, RFDR recoupling and 100 kHz proton decoupling in the 2.4 ms mixing period, and 75 kHz proton decoupling during the evolution and detection periods. Expansions of the CO/C$_\alpha$ crosspeak region from 2D spectra of samples containing 400 μM, 200 μM, and 600 μM DyEDTA are shown in Fig. 5b, c, and d. At 200 μM DyEDTA, cross-

peaks for A57 and L69 are resolved, with ^{13}C NMR linewidths of 2–3 ppm (Fig. 5e), essentially the same as linewidths observed in earlier experiments on fully folded HP35 in frozen solutions at higher temperatures [18]. In our experience, ^{13}C NMR linewidths of approximately 2 ppm are consistently observed in frozen solutions of peptides or proteins that have well-defined molecular conformations at sample temperatures near 150 K [18,28–31]. At higher DyEDTA concentrations (Fig. 5b and d), these crosspeaks merge as the linewidths increase. ^{1}H spin–lattice relaxation rates also increase with increasing DyEDTA concentration, allowing shorter recycle delays in experiments that begin with ^{1}H–^{13}C cross-polarization. Thus, the choice of dopant and concentration can have a strong effect on the quality of the 2D spectra. The experimental results for HP35 suggest that approximately 200 μM DyEDTA may be optimal for monomeric proteins in frozen solutions at 25 K. Effects of dopants on spin relaxation rates are discussed in more detail below.

3.5. Temperature calibration

An important issue for MAS probes is measurement of the sample temperature in the spinning rotor, which may be somewhat different from the temperature measured by a nearby temperature sensor [32]. This is especially important in our low-temperature MAS probe, where different regions of the rotor are exposed to cold helium and to much warmer nitrogen gas. We have developed several different methods for measuring the sample temperature, described in the following paragraphs. As demonstrated in Fig. 2, once NMR signals have been measured at a known temperature, subsequent temperatures can be estimated from the signal amplitudes, provided that thermal equilibrium spin polarizations are established.

Our primary temperature measurement method when setting up experiments is based on the temperature dependence of the spin–lattice relaxation time T_1 for ^{79}Br in KBr. This is a convenient method because a KBr powder sample can then be used both to calibrate the temperature and to adjust the magic angle [33]. Fig. 6 shows T_1 data for both ^{79}Br and ^{81}Br in KBr, measured in a non-spin-
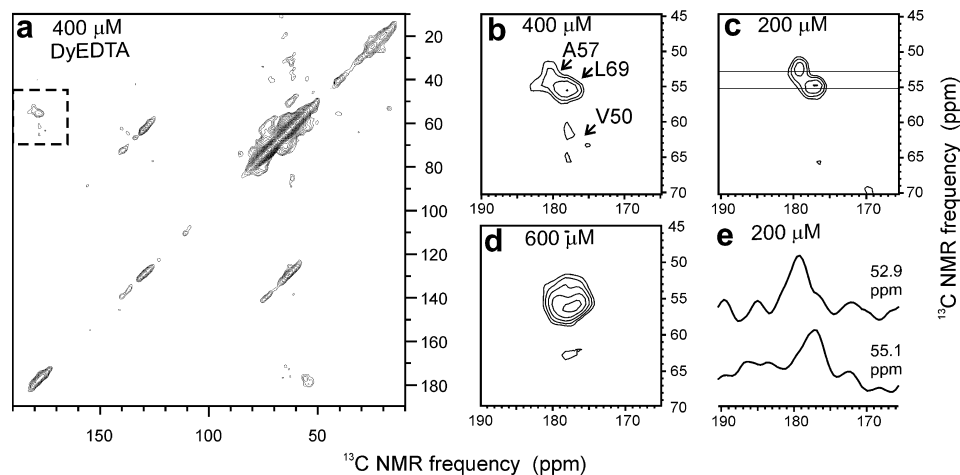
Fig. 5. (a) 2D ^{13}C–^{13}C NMR spectrum of HP35 with 400 µM DyEDTA, acquired with RFDR recoupling in the 2.4 ms mixing period. (b–d) Expansions of CO–C_α crosspeak region for HP35 with 400, 200, and 600 µM DyEDTA, respectively. (e) 1D slices through spectrum with 200 µM DyEDTA at 52.9 and 55.1 ppm. Spectra obtained at 25 K with 6.70 kHz MAS. (For 200 µM DyEDTA: 0.55 mg HP35 in 48 µl glycerol/water (3:2 ratio by volume), ^{1}H T_1 = 5.3 s, recycle delay = 7 s, 2148 total scans. For 400 µM DyEDTA: 0.76 mg HP35 in 48 µl glycerol/water (1:1), ^{1}H T_1 = 3.3 s, recycle delay = 5 s, 2048 total scans. For 600 µM: 0.79 mg HP35 in 48 µl glycerol/water (1:1), ^{1}H T_1 = 3.0 s, recycle delay = 3.75 s, 8192 total scans).
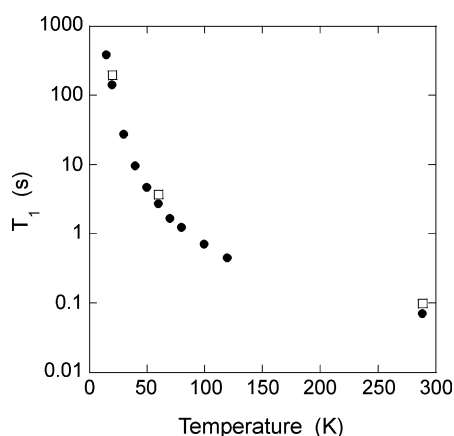

Fig. 6. ^{79}Br (●) and ^{81}Br (□) spin–lattice relaxation time T_1 in KBr powder as a function of temperature. Longer T_1 values for ^{81}Br reflect a quadrupolar relaxation mechanism.

ning helium-cooled probe, based on a customized Janis SuperTran continuous flow cryostat, that provides accurate sample temperatures [5–10]. The relaxation rate is a very strong function of temperature, changing by almost three orders of magnitude from 100 to 15 K. This provides very good temperature sensitivity, especially in the 20–30 K range that is most relevant to our low-temperature MAS experiments. Comparison of ^{79}Br and ^{81}Br T_1 values indicates a quadrupolar, rather than magnetic, relaxation mechanism. The experimental temperature dependence of T_1 for ^{79}Br fits the following empirical expression to within 5% between 20 and 296 K: $T_1 = 0.0145 + 5330T^{-2} + (1.42 \times 10^7)T^{-4} + (2.48 \times 10^9)T^{-6}$.

T_1 values in Fig. 6 were measured by saturation recovery of the central NMR line (20 π/2 pulses with 1, 5, or 10 ms gaps for saturation), using a single-exponential fit. In general, the relaxation of a nucleus with spin >1/2 is not single-exponential, and the relaxation of the central and satellite transitions will be different [34]. However, for KBr under MAS, we have found the T_1 values of the central NMR line and the MAS sidebands to be equal, both at room temperature and 25 K. This is likely because of fast spin exchange between the different transitions across the fairly narrow width (~25 kHz) of the quadrupolar-broadened lineshape. The spin–spin

relaxation time of ^{81}Br is 400 µs at room temperature [35], and we have measured ~200 µs for ^{79}Br at 30 K (non-spinning). Also, our measurements of T_1 at various MAS frequencies near room temperature do not show any dependence on ν_{MAS}, other than effects due to changes of sample temperature with spinning speed. Our T_1 measurements are consistent with previous measurements [35,36], suggesting that T_1 values for KBr are not sensitive to sample preparation or purity.

During initial testing of the MAS unit outside the NMR magnet, other methods of temperature measurement were used. The temperature dependence of the ^{35}Cl nuclear quadrupole resonance (NQR) frequency of NaClO$_3$, measured in the non-spinning probe, is shown in Fig. 7. ^{35}Cl NQR signals can be measured with or without sample rotation, so that the data in Fig. 7 can be used to determine sample temperatures under MAS conditions outside the magnet. As previously described [37], sample rotation induces orientation-dependent splittings in the NQR line of a single crystal due to quantum adiabatic phases, or broadening of the NQR line of a NaClO$_3$ powder. Data in Fig. 7 then apply to the center frequency of the split or broadened NQR lineshape. At temperatures below 100 K, the ^{35}Cl NQR frequency of NaClO$_3$ follows the empirical expression
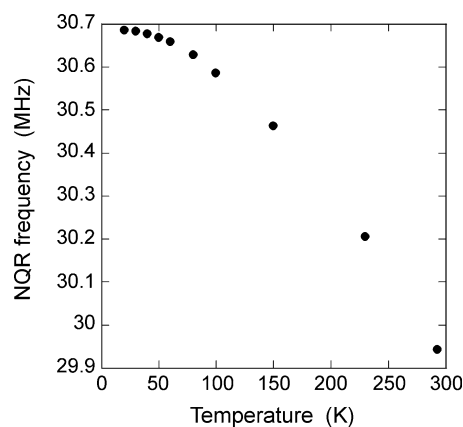

Fig. 7. ^{35}Cl NQR frequency in NaClO$_3$ powder as a function of temperature.

$$\nu_{NQR} = 30.68599\Big\{1.0 - \exp\{-[27393.85919(T^{-1}$$
$$- 0.0022)]^{0.32509}\}\Big\}\ MHz.$$

Under given bearing and drive pressures and a given liquid helium flow rate, sample temperatures can also be estimated outside the NMR magnet by placing a diode temperature sensor (Lake Shore model DT-421) inside the (stationary) rotor. Using this method, we could measure the temperature gradient across the sample region. At a sample center temperature of 27 K, we measured no temperature difference at the drive end, and a 6 K increase at the opposite end of the sample region. According to these measurements, the sample region has a relatively small temperature gradient, despite the large temperature difference between the helium cooling gas and nitrogen bearing gas. Absence of a large temperature gradient is also consistent with the single-exponential nature of T_1 recovery curves.

Possible effects of rf irradiation on the sample temperature were investigated by measuring the ^{79}Br signal amplitude from KBr powder with and without proton decoupling (75 kHz rf field during 20 ms free-induction decays, 2 s recycle delay) at 30 K. No detectable change in signal amplitude (<1%) was observed, indicating that rf heating was less than 0.2 K.

Prior to ^{13}C NMR experiments such as those in Figs. 3–5, 8 and 9, the temperature of a KBr powder sample under given conditions of MAS frequency, MAS bearing pressure, and liquid helium flow rate was first determined from a ^{79}Br T_1 measurement. We then assumed that the temperature of a ^{13}C-containing sample would be the same under the same experimental conditions. Data in Fig. 2 support the validity of this assumption.

3.6. Spin–lattice relaxation times

In some samples, the ^1H and ^{13}C T_1 values can be very long at low temperatures, hurting signal-to-noise by requiring long re-
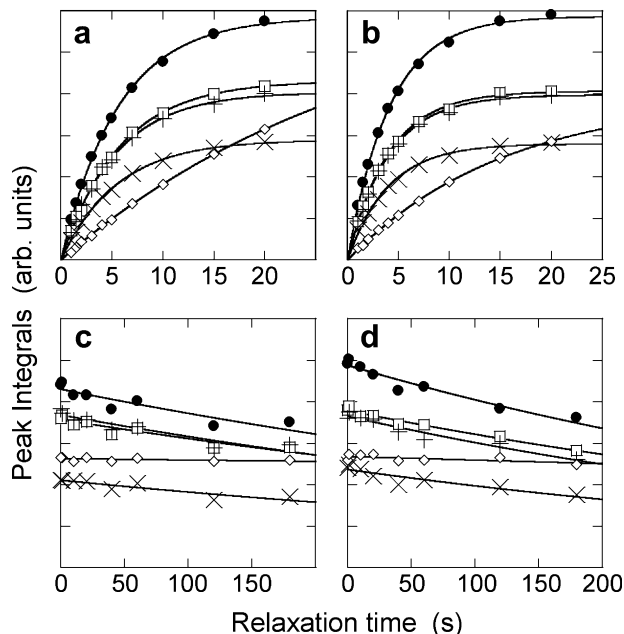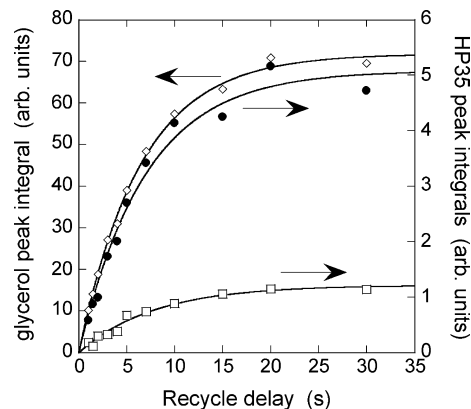

Fig. 9. Recovery of ^1H spin polarization (i.e., ^1H T_1 data) detected through cross-polarized ^{13}C signals as a function of recycle delay in a frozen solution of HP35 in glycerol/water solution with 200 μM DyEDTA at 25 K. Symbols are ● = HP35 $^{13}C_\beta$, $^{13}C_\gamma$, and $^{13}C_\delta$; □ = HP35 ^{13}CO; ◇ = natural-abundance glycerol ^{13}C. Solid lines are fits to exponential recovery curves.

cycle delays. In general, paramagnetic dopants can be added to frozen solutions to reduce the ^1H T_1 [18,29–31]. Several paramagnetic compounds were tested in frozen glycerol/water solutions, as shown in Table 1. Of these compounds, DyEDTA was most effective at low temperatures. In contrast to FeEDTA and CuEDTA, which can be effective as relaxation agents at temperatures above 100 K [18,29–31] but become ineffective at lower temperatures, DyEDTA produces a ^1H T_1 that decreases with decreasing temperature down to at least 25 K. Spectra of HP35 described above indicate that DyEDTA concentrations around 200 μM have only minor effects on ^{13}C MAS NMR linewidths at 25 K.

Measurements of ^1H spin–lattice relaxation by the recovery of cross-polarized ^{13}C signals revealed different behavior in the Aβ$_{14–23}$ and HP35 samples, as shown in Figs. 8 and 9. The ^{13}C NMR signals of Aβ$_{14–23}$ fibrils are associated with a relatively short ^1H T_1 (5.6 ± 0.3 s) at 20 K, even without paramagnetic doping (see Fig. 8). However, signals from natural-abundance ^{13}C of glycerol in the same sample are associated with a much longer ^1H T_1 (∼30 s). Similar behavior is observed in ^{13}C T_1 measurements, performed with the double-resonance technique of Torchia [38]. The ^{13}C T_1 values are much greater than the ^1H T_1 values, but the Aβ$_{14–23}$ ^{13}C signals still decay faster ($T_1 \sim 700$ s) than the glycerol ^{13}C, which has little decay over the longest measurement time of 180 s. When an Aβ$_{14–23}$ fibril sample with 160 μM DyEDTA was used, the ^1H T_1 values were reduced for both the Aβ$_{14–23}$ and the glycerol ^{13}C NMR signals, but the T_1 values for Aβ$_{14–23}$ were still much shorter. In the case of HP35 in a DyEDTA-doped glycerol/water solution, the ^1H T_1 values associated with HP35 and glycerol signals are the same within experimental uncertainty. For a sample with 200 μM DyEDTA (Fig. 9), the ^1H T_1 values are 6.5 ± 0.5 s for

Fig. 8. Recovery of ^1H spin polarization (i.e., ^1H T_1 data) detected through cross-polarized ^{13}C NMR signals as a function of recycle delay in a frozen solution of Aβ$_{14–23}$ fibrils in glycerol/water without paramagnetic dopant at 20 K (a) and with 160 μM DyEDTA at 25 K (b). Decay of ^{13}C spin polarization (i.e., ^{13}C T_1 data) as a function of relaxation time for the same samples without dopant (c) and with dopant (d). Symbols are ● = V18 $^{13}C_\gamma$ and A21 $^{13}C_\beta$; □ = V18 and A21 ^{13}CO; + = V18 $^{13}C_\beta$; × = A21 $^{13}C_\alpha$; ◇ = natural-abundance glycerol ^{13}C. Solid lines are fits to exponential recovery (a and b) and decay (c and d) curves.

Table 1
Paramagnetic dopants tested for low-temperature relaxation in frozen glycerol/water solutions

Dopant	Concentration (mM)	Temperature (K)	^1H T_1 (s)
DyEDTA	0.2	25	5.4
DyDOTA	1	∼25	18
EuEDTA	10	∼25	10
FeEDTA	15	∼70	1.8
FeEDTA	15	∼40	5
CuEDTA	15	∼70	13
CuEDTA	15	∼40	31

^1H T_1 values were detected through cross-polarized glycerol ^{13}C signals as a function of the recycle delay.

glycerol, and 7.1 ± 1.5 s for the HP35 signals resolved from glycerol in the 1D spectrum.

Apparent differences in spin–lattice relaxation behavior in the two samples may result from intrinsic differences in molecular motions (e.g., methyl rotations). Alternatively, these differences may be a result of the fact that the HP35 solution has a relatively low concentration of individual protein molecules surrounded by the glycerol/water solvent, which allows ^{1}H spin diffusion to average out differences in the intrinsic ^{1}H T_1 values of the protein and the solvent. In contrast, the suspension of $A\beta_{14-23}$ fibrils in glycerol/water is visibly milky, indicating the presence of fibril clumps in which the local concentration of $A\beta_{14-23}$ molecules is high (on the order of 1 M within an amyloid fibril [39,40]) over length scales greater than 100 nm. Given that ^{1}H spin diffusion constants are roughly 600 nm^2 s^1 [41], equalization of ^{1}H spin polarizations over 100 nm length scales takes roughly 30 s. Thus, it is not surprising that ^{1}H T_1 values detected through ^{13}C NMR signals of $A\beta_{14-23}$ fibrils and glycerol are different under our experimental conditions. Moreover, the data in Fig. 8 indicate that the intrinsic ^{1}H T_1 in $A\beta_{14-23}$ fibrils is approximately 6 s at 20 K. The intrinsic ^{1}H T_1 in HP35 may be similar, but is not observable in a dilute, monomeric HP35 solution because spin diffusion equalizes the ^{1}H T_1 values in such a solution and because approximately 99% of the ^{1}H nuclei in the solution belong to solvent molecules (which have intrinsically long T_1 values).

4. Discussion

The experimental results in Figs. 2–5 demonstrate that double-resonance MAS NMR measurements of the type that are commonly employed in structural studies of biomolecular systems can be performed with the probe in Fig. 1 at temperatures around 25 K. This probe has good MAS stability and can achieve sufficiently high rf field strengths (130 kHz for at least 5 ms and 75 kHz for longer periods on the ^{1}H channel; 50 kHz for cross-polarization and dipolar recoupling on the ^{13}C channel) and sufficiently high MAS frequencies (7.00 kHz at 25 K) for a wide variety of useful measurements. The sensitivity advantage of this probe is demonstrated by the data in Fig. 2 and by the observation in Fig. 5 that meaningful 2D ^{13}C–^{13}C NMR spectra of 0.14 μmol of a protein with 2–3 ppm linewidths can be obtained in about 4 h. For comparison, previously reported experiments on ^{13}C-labeled proteins in frozen solutions, performed with commercial MAS probes at roughly 150 K in 9.4 T fields, used 0.25 μmol and 90 h [29] or 1.2 μmol and 96 h [18].

Liquid helium consumption with the current probe design is approximately 3 L/h. While this level of helium consumption may be problematic in some situations, it is not prohibitive in our own laboratory. Recovery and subsequent liquidisation of used helium gas may be possible with a design similar to that in Fig. 1, provided that separation of helium and nitrogen gases is carried out first. In a future probe design, we will attempt to reduce liquid helium consumption and further improve sensitivity by cooling the entire head of the probe, including the drive and bearing gas lines and the rf circuitry, with cold nitrogen gas. For comparison of the liquid helium required for cooling versus the gas required for spinning, we measured experimentally the MAS gas flow. If room temperature helium gas is used for bearing and drive (instead of nitrogen), this probe requires 6 m^3/hr of helium gas (equivalent to 9 L/h of liquid helium). If helium bearing gas is cooled to 77 K before entering the probe, 11 m^3/h of helium gas is required (equivalent to 15 L/h of liquid helium).

In the probe design described here, we have chosen to maintain a relatively large sample volume (48–82 μl, depending on rotor wall thickness), thus precluding high-speed MAS. This is because

our intended applications for this probe involve monomeric proteins in glycerol/water solutions and membrane-associated proteins in multilamellar phospholipid bilayer dispersions. Signal-to-noise in these applications is limited more by the protein concentrations that can be achieved in scientifically relevant samples than by the quantities of isotopically labeled protein that we can produce. In other applications, for example in studies of amyloid fibril structure where very high protein concentrations are scientifically relevant [42], smaller sample volumes and higher MAS frequencies would most likely be preferred.

Our experiments with paramagnetic dopants suggest that DyEDTA is a good choice near 25 K, producing reasonably short ^{1}H T_1 values in glycerol/water at concentrations where paramagnetic line broadening is not severe. ^{13}C line broadening effects may depend on the protein molecular weight or other protein properties. Results in Fig. 8 suggest that amyloid fibrils and similar samples with high local protein concentrations may not require paramagnetic dopants near 25 K. It remains to be determined whether low-temperature MAS experiments on microcrystalline proteins or membrane-associated systems require or benefit from paramagnetic doping.

Finally, a design similar to that in Fig. 1 is likely to be compatible with dynamic nuclear polarization (DNP), which has been shown to produce very large additional sensitivity enhancements in ^{13}C MAS NMR of frozen solutions [43]. In particular, DNP enhancements may increase significantly with decreasing sample temperature in the 20–100 K range [44], possibly allowing large enhancements to be achieved with relatively low microwave powers.

Acknowledgments

Appendix A. Supplementary data

Supplementary data associated with this article can be found, in the online version, at doi:10.1016/j.jmr.2008.09.015.

References

[1] P.L. Kuhns, S.H. Lee, C. Coretsopoulos, P.C. Hammel, O. Gonen, J.S. Waugh, A low-temperature NMR probe for use in a dilution refrigerator, Rev. Sci. Instrum. 62 (1991) 2159–2162.
[2] J.S. Waugh, O. Gonen, P. Kuhns, Fourier-transform NMR at low temperatures, J. Chem. Phys. 86 (1987) 3816–3818.
[3] D.I. Hoult, R.E. Richards, The signal-to-noise ratio of the nuclear magnetic resonance experiment, J. Magn. Reson. 24 (1976) 71–85.
[4] H. Kovacs, D. Moskau, M. Spraul, Cryogenically cooled probes: a leap in NMR technology, Prog. Nucl. Magn. Reson. Spectrosc. 46 (2005) 131–155.
[5] C.A. Michal, R. Tycko, Stray-field NMR imaging and wavelength dependence of optically pumped nuclear spin polarization in InP, Phys. Rev. B 60 (1999) 8672–8679.
[6] R. Tycko, Optical pumping in indium phosphide: ^{31}P NMR measurements and potential for signal enhancement in biological solid state NMR, Solid State Nucl. Mag. 11 (1998) 1–9.
[7] S.E. Barrett, G. Dabbagh, L.N. Pfeiffer, K.W. West, R. Tycko, Optically pumped NMR evidence for finite-size skyrmions in GaAs quantum wells near Landau-level filling $v = 1$, Phys. Rev. Lett. 74 (1995) 5112–5115.
[8] R. Tycko, S.E. Barrett, G. Dabbagh, L.N. Pfeiffer, K.W. West, Electronic states in gallium arsenide quantum wells probed by optically pumped NMR, Science 268 (1995) 1460–1463.
[9] R. Tycko, G. Dabbagh, M.J. Rosseinsky, D.W. Murphy, A.P. Ramirez, R.M. Fleming, Electronic properties of normal and superconducting alkali fullerides

probed by ^{13}C nuclear magnetic resonance, Phys. Rev. Lett. 68 (1992) 1912–1915.

[10] R. Tycko, G. Dabbagh, R.M. Fleming, R.C. Haddon, A.V. Makhija, S.M. Zahurak, Molecular dynamics and the phase transition in solid C_{60}, Phys. Rev. Lett. 67 (1991) 1886–1889.

[11] M. Linder, A. Hohener, R.R. Ernst, Proton-enhanced carbon-13 resonance in a helium-cooled probe: chemical shielding tensor of benzene, J. Magn. Reson. 35 (1979) 379–386.

[12] A. Hackmann, H. Seidel, R.D. Kendrick, P.C. Myhre, C.S. Yannoni, Magic-angle spinning NMR at near-liquid-helium temperatures, J. Magn. Reson. 79 (1988) 148–153.

[13] D.A. Hall, D.C. Maus, G.J. Gerfen, S.J. Inati, L.R. Becerra, F.W. Dahlquist, R.G. Griffin, Polarization-enhanced NMR spectroscopy of biomolecules in frozen solution, Science 276 (1997) 930–932.

[14] A. Samoson, T. Tuherm, J. Past, A. Reinhold, T. Anupold, I. Heinmaa, New horizons for magic-angle spinning NMR, Top. Curr. Chem. 246 (2005) 15–31.

[15] M. Carravetta, A. Danquigny, S. Mamone, F. Cuda, O.G. Johannessen, I. Heinmaa, K. Panesar, R. Stern, M.C. Grossel, A.J. Horsewill, A. Samoson, M. Murata, Y. Murata, K. Komatsu, M.H. Levitt, Solid state NMR of endohedral hydrogen-fullerene complexes, Phys. Chem. Chem. Phys. 9 (2007) 4879–4894.

[16] V. Macho, R. Kendrick, C.S. Yannoni, Cross polarization magic-angle spinning NMR at cryogenic temperatures, J. Magn. Reson. 52 (1983) 450–456.

[17] Z. Bu, Y. Shi, D.J.E. Callaway, R. Tycko, Molecular alignment within β-sheets in $A\beta_{14-23}$ fibrils: solid state NMR experiments and theoretical predictions, Biophys. J. 92 (2007) 594–602.

[18] R.H. Havlin, R. Tycko, Probing site-specific conformational distributions in protein folding with solid state NMR, Proc. Natl. Acad. Sci. USA 102 (2005) 3284–3289.

[19] C.J. McKnight, P.T. Matsudaira, P.S. Kim, NMR structure of a highly thermostable subdomain within villin headpiece, J. Cell. Biochem. 59 (1995) 49.

[20] T.K. Chiu, J. Kubelka, R. Herbst-Irmer, W.A. Eaton, J. Hofrichter, D.R. Davies, High-resolution x-ray crystal structures of the villin headpiece subdomain, an ultrafast folding protein, Proc. Natl. Acad. Sci. USA 102 (2005) 7517–7522.

[21] A.E. Bennett, C.M. Rienstra, J.M. Griffiths, W.G. Zhen, P.T. Lansbury, R.G. Griffin, Homonuclear radio-frequency-driven recoupling in rotating solids, J. Chem. Phys. 108 (1998) 9463–9479.

[22] A.E. Bennett, C.M. Rienstra, M. Auger, K.V. Lakshmi, R.G. Griffin, Heteronuclear decoupling in rotating solids, J. Chem. Phys. 103 (1995) 6951–6958.

[23] A.B. Siemer, C. Ritter, M. Ernst, R. Riek, B.H. Meier, High-resolution solid state NMR spectroscopy of the prion protein HET-s in its amyloid conformation, Angew. Chem. Int. Ed. 44 (2005) 2441–2444.

[24] R.W. Martin, K.W. Zilm, Preparation of protein nanocrystals and their characterization by solid state NMR, J. Magn. Reson. 165 (2003) 162–174.

[25] A.K. Paravastu, R. Tycko, Frequency-selective homonuclear dipolar recoupling in solid state NMR, J. Chem. Phys. 124 (2006) 194303.

[26] M. Hohwy, H.J. Jakobsen, M. Eden, M.H. Levitt, N.C. Nielsen, Broadband dipolar recoupling in the nuclear magnetic resonance of rotating solids: a compensated C7 pulse sequence, J. Chem. Phys. 108 (1998) 2686–2694.

[27] M.S. Lehmann, T.F. Koetzle, W.C. Hamilton, Precision neutron diffraction structure determination of protein and nucleic acid components. I. The crystal and molecular structure of the amino acid L-alanine, J. Am. Chem. Soc. 94 (1972) 2657–2660.

[28] S. Sharpe, W.M. Yau, R. Tycko, Structure and dynamics of the HIV-1 Vpu transmembrane domain revealed by solid state NMR with magic-angle spinning, Biochemistry 45 (2006) 918–933.

[29] S. Sharpe, N. Kessler, J.A. Anglister, W.M. Yau, R. Tycko, Solid state NMR yields structural constraints on the V3 loop from HIV-1 gp120 bound to the 447–52d antibody Fv fragment, J. Am. Chem. Soc. 126 (2004) 4979–4990.

[30] D.P. Weliky, A.E. Bennett, A. Zvi, J. Anglister, P.J. Steinbach, R. Tycko, Solid state NMR evidence for an antibody-dependent conformation of the V3 loop of HIV-1 gp120, Nat. Struct. Biol. 6 (1999) 141–145.

[31] H.W. Long, R. Tycko, Biopolymer conformational distributions from solid state NMR: α-helix and 3_{10}-helix contents of a helical peptide, J. Am. Chem. Soc. 120 (1998) 7039–7048.

[32] A. Bielecki, D.P. Burum, Temperature dependence of ^{207}Pb MAS spectra of solid lead nitrate. An accurate, sensitive thermometer for variable temperature MAS, J. Magn. Reson. A 116 (1995) 215–220.

[33] J.S. Frye, G.E. Maciel, Setting the magic angle using a quadrupolar nuclide, J. Magn. Reson. 48 (1982) 125–131.

[34] E.R. Andrew, D.P. Tunstall, Spin–lattice relaxation in imperfect cubic crystals and in non-cubic crystals, Proc. Phys. Soc. 78 (1961) 1–11.

[35] T.K. Halstead, P.A. Osment, B.C. Sanctuary, J. Tegenfeldt, I.J. Lowe, Multipole NMR. VII. Bromine NMR quadrupolar echoes in crystalline KBr, J. Magn. Reson. 67 (1986) 267–306.

[36] E.G. Wikner, W.E. Blumberg, E.L. Hahn, Nuclear quadrupole spin–lattice relaxation in alkali halides, Phys. Rev. 118 (1960) 631–639.

[37] R. Tycko, Adiabatic rotational splittings and Berry's phase in nuclear quadrupole resonance, Phys. Rev. Lett. 58 (1987) 2281–2284.

[38] D.A. Torchia, Measurement of proton-enhanced ^{13}C T_1 values by a method which suppresses artifacts, J. Magn. Reson. 30 (1978) 613–616.

[39] S. Luca, W.M. Yau, R. Leapman, R. Tycko, Peptide conformation and supramolecular organization in amylin fibrils: constraints from solid state NMR, Biochemistry 46 (2007) 13505–13522.

[40] A.T. Petkova, W.M. Yau, R. Tycko, Experimental constraints on quaternary structure in Alzheimer's β-amyloid fibrils, Biochemistry 45 (2006) 498–512.

[41] D.L. VanderHart, G.B. McFadden, Some perspectives on the interpretation of proton NMR spin diffusion data in terms of polymer morphologies, Solid State Nucl. Mag. 7 (1996) 45–66.

[42] R. Tycko, Molecular structure of amyloid fibrils: insights from solid state NMR, Q. Rev. Biophys. 39 (2006) 1–55.

[43] T. Maly, G.T. Debelouchina, V.S. Bajaj, K.N. Hu, C.G. Joo, M.L. Mak-Jurkauskas, J.R. Sirigiri, P.C.A. van der Wel, J. Herzfeld, R.J. Temkin, R.G. Griffin, Dynamic nuclear polarization at high magnetic fields, J. Chem. Phys. 128 (2008) 052211.

[44] K.-N. Hu, Ph.D. Thesis, Department of Chemistry, Massachusetts Institute of Technology, 2006.